This article is a non-peer reviewed EarthArXiv preprint.

Verifying pore network models of imbibition in rocks using time-resolved synchrotron imaging

Tom Bultreys[1,2], Kamaljit Singh[1], Ali Q. Raeini[1], Leonardo C. Ruspini[3], Pål-Eric Øren[3], Steffen Berg[4], Maja Rücker[5], Branko Bijeljic[1], Martin J. Blunt[1]

[1]Department of Earth Science and Engineering, Imperial College London, London, SW7 2AZ, United Kingdom

[2]UGCT/PProGRess, Dept. of Geology, Ghent University, Belgium

[3]Petricore Norway AS, Trondheim, Norway

[4]Shell Global Solutions BV, Amsterdam, The Netherlands

[5]Department of Chemical Engineering, Imperial College London, United Kingdom

Key Points:

- A new method to compare pore network simulations of two-phase flow to time-resolved micro-CT data
- Evolution of fluid distributions were validated with respect to pore size, connectivity and flow paths
- Quasi-static pore network models put the fluids in approximately the right pores to predict flow properties

Corresponding author: Tom Bultreys, Tom.Bultreys@UGent.be

Abstract

At the pore scale, slow invasion of a wetting fluid in porous materials is often modelled with quasi-static approximations which only consider capillary forces in the form of simple pore filling rules. The appropriateness of this approximation, often applied in pore network models, is contested in literature, reflecting the difficulty of predicting imbibition relative permeability with these models. However, validation by sole comparison to continuum-scale experiments is prone to induce model overfitting. It has therefore remained unclear whether difficulties generalizing the model performance are due to network extraction, the pore filling rules, or whether a quasi-static description is useful at all. Here, we address this by examining whether such a model can predict the pore-scale fluid distributions underlying the behaviour at the continuum scale. To this end, we compare the fluid arrangement evolution measured in fast synchrotron micro-CT experiments on two rock types to quasi-static simulations which implement capillary-dominated pore filling and snap-off, including a sophisticated model for cooperative pore filling. The results indicate that pore network models with appropriate pore filling rules can in principle obtain a good first-order prediction of the upscaled flow properties of strongly-wetted rocks at low capillary numbers.

1 Introduction

Dunking a biscuit into tea, which then soaks up the liquid, is an everyday example of a wetting fluid (tea) displacing a non-wetting fluid (air) in a porous medium (biscuit). This process, termed imbibition, occurs in nature in the topmost layer of soil during rainfall, during the flow of immiscible pollutants in ground water resources, the geological storage of carbon dioxide or hydrogen, and the management of petroleum reservoirs [*Bickle*, 2009; *Atteia et al.*, 2013; *Blunt*, 2017]. To understand the link between pore structure, wettability and upscaled multi-phase flow parameters, a large amount of effort has been put into simulating the pore-scale fluid distribution and calculating the corresponding macroscopic properties [*Meakin and Tartakovsky*, 2009; *Bultreys et al.*, 2016a].

The key challenge in this field is to describe the intricate arrangement of the two fluids in the pore space during the fluid invasion [*Herring et al.*, 2013; *Armstrong et al.*, 2016; *Zhao et al.*, 2016]. Models struggle to capture the effect of the many fluid-fluid interface movements on the fluid flow over sufficiently large length and time scales [*Meakin and Tartakovsky*, 2009]. While Navier-Stokes solvers are becoming mature enough to perform useful numerical experiments on domains tens of pores across over relatively short time scales [*Fer-*

rari and Lunati, 2013; *Shams et al.*, 2018; *Alpak et al.*, 2018; *McClure et al.*, 2018], it remains desirable to define a more conceptual model which describes the emergence of structures at the scale of fluid clusters for upscaling [*Hilfer et al.*, 2015].

Pore network models (PNMs) conceptualize the pore space as a network of larger void volumes, pores, bounded by restrictions, called throats (Figure 2). In Earth science cases, the global flow rates are typically so low that the capillary force is often assumed to be dominant at the pore scale [*Blunt*, 2017]. The most computationally efficient type of pore network models therefore adopts the quasi-static assumption: only capillary forces are taken into account and the fluids are assumed in capillary quasi-equilibrium at each moment [*Wilkinson and Willemsen*, 1983; *Blunt et al.*, 1992]. The fluid invasion process is abstracted into filling rules which aim to produce similar emerging fluid distribution patterns as when the capillary, viscous and inertial forces drive the process in reality [*Blunt et al.*, 2013]. The pore space is invaded as a sequence of invasion events of three types: snap-off, piston-like displacement and cooperative pore filling [*Lenormand et al.*, 1983]. Predicting the evolution of the pore-scale fluid distribution therefore reduces to calculating the entry capillary pressure for each of these events in all available pores, and gradually filling the pore space with the invading fluid in order of this pressure. Dynamic pore network models, on the other hand, explicitly capture the visco-capillary force balance of immiscible transport [*Lenormand et al.*, 1983; *Joekar-Niasar and Hassanizadeh*, 2012], but come at the price of increased complexity and computational demands.

While a number of early studies have showed that quasi-static PNMs can match experimental relative permeability curves in specific cases [*Øren et al.*, 1998; *Valvatne and Blunt*, 2004; *Blunt et al.*, 2013], substantial efforts over several decades have not led to satisfying predictive capabilities in a general sense [*Bondino et al.*, 2012]. It has been unclear whether the shortcomings originate from uncertainties in the extracted network, the pore filling rules, or whether it is adequate to use a quasi-static description at all. Newly available fast time-resolved X-ray micro-CT experiments [*Wildenschild and Sheppard*, 2013; *Youssef et al.*, 2013; *Berg et al.*, 2013; *Andrew et al.*, 2015; *Bultreys et al.*, 2016b; *Schlüter et al.*, 2017; *Singh et al.*, 2017] have challenged the quasi-static assumption, as viscous and inertial effects such as ganglion dynamics and intermittency have been observed [*Rücker et al.*, 2015; *Armstrong et al.*, 2016; *Gao et al.*, 2017; *Reynolds et al.*, 2017]. However, it is currently not well understood how strongly the quasi-static approximation deviates from the experimental reality in rock samples, and if this produces fundamentally flawed predictions at the intermediate

scale of the fluid clusters. The validation question is complicated by the fact that model simplifications lead to a large number of internal microscopic degrees of freedom, but the output consists of relatively few macroscopic parameters that can be used for validation. Therefore, there is a risk of overfitting the model when tuning it to experimentally measured continuum scale flow properties, e.g. relative permeability and capillary pressure-saturation functions [*Bondino et al.*, 2012; *Aghaei and Piri*, 2015; *Masalmeh et al.*, 2015; *Jerauld et al.*, 2017]. Instead, criteria which contain enough information to reconstruct the relevant aspects of the system's internal state are required [*Liu et al.*, 2013].

In a previous study, we showed how PNM predictions can be mapped to fluid distributions measured with micro-CT to facilitate direct pore-by-pore comparisons [*Bultreys et al.*, 2018]. Here, we extend this to time-resolved micro-CT datasets to validate the filling sequence rather than a static snap-shot, resulting in a more complete picture. The experimental data in this study are two publicly available fast synchrotron micro-CT datasets of water-flooding in strongly water-wet Ketton limestone [*Singh et al.*, 2017] and Gildehauser sandstone [*Rücker et al.*, 2015]. This study investigates whether a quasi-static assumption can result in realistic filling sequences for strong imbibition at low capillary numbers. Contrary to previous studies, e.g. *Berg et al.* [2016], the models used here implement snap-off and cooperative pore filling processes on experimentally based geometries [*Valvatne and Blunt*, 2004; *Ruspini et al.*, 2017]. We used a realistic cooperative pore filling algorithm [*Ruspini et al.*, 2017], and minimized the influence of the specific PNM extraction and of the boundary conditions on the analysis. The general workflow is depicted in figure 1. We find that the quasi-static model generally puts the fluids in the right pores to approximate mm-scale averaged properties, at least in strongly water-wet samples at low capillary numbers.

2 Materials and methods

2.1 Experiments

Details of the Ketton and Gildehauser unsteady-state (constant injection flow rate) imbibition experiments are described in *Singh et al.* [2017] and *Rücker et al.* [2015]. Both datasets are publicly available [*Singh et al.*, 2018; *Berg et al.*, 2018]. Ketton and Gildehauser (the latter a local variety of Bentheimer) respectively have a porosity of 23 % and 20 %; and a permeability of 2.8×10^{-12} m^2 and 1.48×10^{-12} m^2 [*Andrew et al.*, 2014]. In the experiments, KI-brine was used as the wetting phase and decane as the non-wetting phase. As the

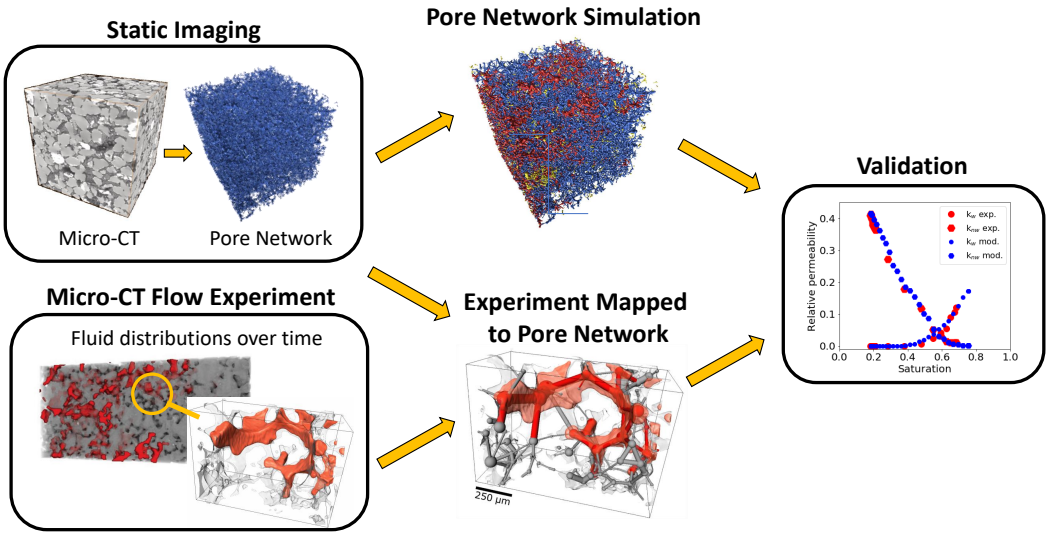

Figure 1. The workflow for validation of pore scale multi-phase flow models proposed in this paper. After extracting a pore network model from a micro-CT scan of the sample, we generated a series of fluid distributions in the pore network model by either numerical simulation or experimental micro-CT imaging. We then investigate whether the simulation succeeds at filling pores in approximately the right order compared to the experiment, particularly with regards to predicting upscaled flow properties.

samples were clean quarry stones, they were water-wet. Cylindrical samples with a diameter of approximately 4 mm and a height of 10 mm were inserted into flow cells. First, a high quality dry micro-CT scan was obtained. Next, the samples were fully saturated with brine and drained by injecting decane. Then, imbibition was initiated by injecting brine at very low capillary numbers (1.26×10^{-9} in the Ketton case, 1.8×10^{-8} in the Gildehauser case). During imbibition, each sample was partly imaged along its height by fast micro-CT (Ketton: 400 scans at 38 seconds/scan, voxel size 3.28 μm, image height 3.28 mm; Gildehauser: 40 scans at 45 seconds/scan, voxel size 4.4 μm, image height 2.49 mm). Imaging was performed at I13-2 (Diamond Light Source) and at TOMCAT (Swiss Light Source). As detailed in the aforementioned references, the images were treated with a non-local means filter and segmented with the watershed algorithm in Avizo 9 (ThermoFisher/FEI). The final Gildehauser image contained an oil cluster connected to the top and the bottom of the image, i.e. the oil in the sample may still have been mobile.

2.2 Quasi-static modelling

The pore network models used here were extracted from the segmented dry scans using the maximal ball method [*Raeini et al.*, 2017]. This method employs the distance map of the pore space image to find pores and throats as constrictions and dilations. The radii of these elements were found by looking for the maximum inscribed spheres at these locations. Shape factors were used to describe the angularity of pores and throats as described in *Bultreys et al.* [2018]. The pores and throats had circular, triangular and square cross-sections, based on their shape factor [*Valvatne and Blunt*, 2004].

After network extraction, imbibition was simulated using a quasi-static invasion percolation approach, based on *Øren et al.* [1998], *Valvatne and Blunt* [2004] and *Ruspini et al.* [2017]. Following these works, entry pressures were calculated for each pore and throat which could be accessed by the invading fluid and from which the defending fluid had an escape path (i.e. was not trapped). The pressure calculations are summarized in the Supporting Information. The wetting phase was injected from the top and bottom face, and the non-wetting phase was allowed to escape through both, to account for backflow in the porous medium outside the field of view. We used the fluid occupancy at the start of imbibition in the experimental data to assign the initial condition of the model. Advancing contact angles were randomly assigned to each pore or throat in the range between 35 and 45 degrees for Ketton [*Scanziani et al.*, 2017] and 35 and 55 degrees for Gildehauser [*Khishvand et al.*, 2016], based on in situ contact angle measurements. We list here the PNM assumptions and parameters which can influence the simulated filling sequence:

- The segmentation of the micro-CT scan. While this can have an important effect on the network extraction and simulations, the large pores and the good image quality in the dry scans was deemed to lead to high quality segmentations. We used the segmented images provided in the public domain data sets, without tuning the segmentation to improve the PNM results.
- The detection of pore and throat centres as local minima and maxima of the distance map. The main user-defined parameter is the minimum inscribed radius for a point to be called a pore centre, set to 1.5 voxel lengths. This does not affect the results for the well-resolved, rather simple pore structures in this work. In any event, the same network extraction was used to analyse both the experiment and the model.

- Pore and throat shape factor determination, and the simplification of pore shapes to (predominantly) triangles with the same shape factor and inscribed radius [*Øren et al.*, 1998]. This induces an approximation, but it is fully defined by the detection of pore centres and throat surfaces.
- Advancing contact angle assignment. These were randomly assigned in each pore or throat in the range between 35 degrees and 45 degrees for Ketton [*Singh et al.*, 2016; *Scanziani et al.*, 2017] and 35 degrees and 55 degrees for Gildehauser [*Khishvand et al.*, 2016], based on in situ contact angle measurements. The sensitivity within likely values (several ranges spanning 25 degrees to 65 degrees) was found not to influence the conclusions in this paper, as shown in the Supporting Information.
- The capillary pressure reached during drainage, prior to imbibition. This is inferred from the radius of the smallest pore or throat that is oil-filled in the micro-CT image after drainage.
- One parameter in the cooperative pore filling algorithm, which determines when the interface becomes unstable while entering the throats. This parameter has a very limited influence on the simulations results [*Ruspini et al.*, 2017].

2.3 Data analysis

To allow consistent comparison of the experiments to PNM simulations, we used the PNM as an image analysis tool on the imbibition datasets. As detailed in *Bultreys et al.* [2018], the inscribed spheres at each pore and throat centre in the dry scan were determined during network extraction. These were used to define the fluid occupying the pore or throat centre. For each time step in the imbibition experiment, a pore or throat was called wetting-filled if more than half of the voxels of the associated inscribed sphere are segmented as wetting fluid. The simulations were run on the same PNM used to analyse the experiments, enabling a like-for-like comparison (Figure 2). The measures shown in this paper were calculated on the PNM structure, with fluid distributions mapped from the experiments, or from simulations on the PNM.

2.3.1 Filling size

Pores and throats in the experiment were considered to be invaded at time step t if they were filled with wetting fluid in image t and with non-wetting fluid in image $t-1$. If they

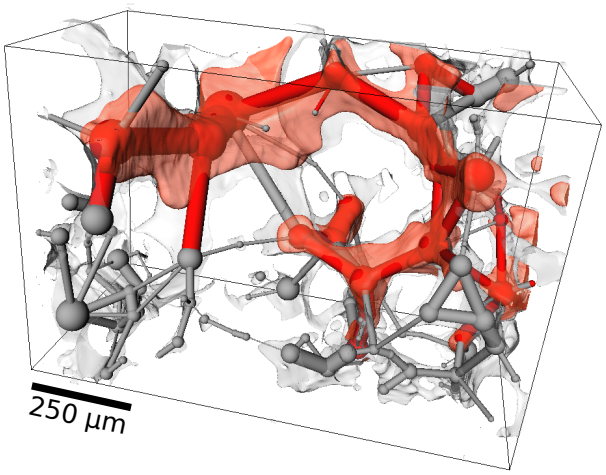

Figure 2. Voids in Ketton limestone, with the non-wetting fluid observed in one of several hundred snapshots of an imbibition experiment indicated in transparent red (the figure shows a small subvolume of a micro-CT scan). The balls and sticks represents the corresponding pore network model, colored according to the fluids occupying each pore or throat in a simplified model of fluid invasion. We use this one-to-one mapping to compare the evolving fluid filling pattern to the experiment.

changed filling state more than 3 times, they were not listed here, as these were a small number of mainly narrow throats affected by image noise. The filling time was then translated to the filling sequence rank number (the rank of the pore or throat filling event when ordered according to the filling time). This was necessary because the simulations do not have a time scale, but only predict in which order pores and throats fill. In the Gildehauser case, the rate of filling was relatively large compared to the time resolution of the imaging. Therefore, filling sizes at certain time steps in this experiment are shown using box plots with outliers.

2.3.2 Connectivity

To characterize the connectivity, we calculate the Euler characteristic of the shape formed by the throats (conceptualized here as cylinders) and pores (conceptualized as spheres) that are filled with the non-wetting phase from either the experiment or the simulation. We first remove isolated non-wetting phase-filled throats to reduce the dependency on imaging noise. Then, we modify this shape by adding a sphere to the end of any cylinder which does not already end in a sphere. This does not change the Euler characteristic as it is invariant under continuous deformation of the shape. The Euler characteristic χ can be calculated us-

ing the Betti numbers β_i:

$$\chi = \beta_0 - \beta_1 + \beta_2 \tag{1}$$

Here, β_0 equals the number of connected components k and β_2 is the number of holes in the shape, the latter by construction equaling zero. β_1 is the number of loops in the shape [*Wildenschild and Sheppard*, 2013], equalling $N_e - N_v + k$, with N_e the number of edges and N_v the number of vertices of the corresponding graph [*Berge*, 2001]. Therefore, the calculation of the Euler characteristic reduces to:

$$\chi = N_v - N_e \tag{2}$$

Note that the calculation does not depend on the exact pore and throat shapes. Detecting the connected components in the non-wetting phase graph allows to calculate the amount and sizes of clusters, after which the amount of loops can be calculated as $k - \chi$.

2.3.3 Flow paths

The relevance of discrepancies in the filling sequence to relative permeabilities is a question of key concern [*Berg et al.*, 2016]. However, the calculation of volumes and fluid flow conductances for each pore and throat induces non-uniqueness associated with user-defined parameters [*Sorbie and Skauge*, 2011]. Since we are only interested here in the fluid displacements and not in improving conductivity or saturation calculations, we circumvent this problem by calculating relative permeabilities for both the experimental and the simulated fluid distributions on the same PNM, using the same (possibly imprecise) conductivities and volumes. This yields a flow-weighted connectivity metric which is a proxy to (but not necessarily equal to) physical relative permeability measurements.

For the experiments, relative permeabilities were calculated by mapping the experimentally observed fluid distribution on the same PNM as used in the imbibition simulations. The Hagen-Poiseuille conductivity model was used to calculate the flow rates through the wetting and the non-wetting phase separately, using the OpenPNM pore network modelling package [*Gostick et al.*, 2016]. We assumed that throats filled with one phase have zero conductivity for the other phase. Flow rates for the simulations were calculated on the same PNM with the same conductivities, and discrepancies compared to the experiment therefore came solely from differences in the fluid distribution. A good match means the flow distribution in the model is approximately correct to predict the upscaled properties. However, to

match experimentally measured relative permeabilities (based on pressure measurements), it may still be necessary to improve the volume and conductivity assignment of pores and throats. This less fundamental issue is outside the scope of the study.

Results and discussion

Previous studies have shown that the pore-scale fluid distribution in experiments is not fully reproducible [*Ferrari et al.*, 2015; *Ling et al.*, 2017; *Bultreys et al.*, 2018]. The averaged properties are, however, much more reproducible, as different realisations of the fluid distribution can lead to consistent averaged results if they are statistically similar. Therefore, simply comparing the filling sequence on a pore-by-pore basis does not offer a relevant answer [*Bultreys et al.*, 2018]. Recognizing that a good prediction of the upscaled multi-phase flow properties needs to capture the geometry and the connectivity of the fluid phases throughout the filling sequence, we use the following criteria to validate the model:

- In terms of size (radius), which pores and throats are filled throughout the filling sequence?
- How does the connectivity of the non-wetting phase change during the filling sequence?
- How do the flow paths of the wetting and the non-wetting phase change throughout the filling sequence?

As our goal was to evaluate physical concepts rather than model implementation, the influence of PNM non-uniqueness on the validation was reduced as much as possible. Parameters that affect the filling sequence were set based on physical principles and were sensitivity-checked.

Filling size

The PNM used in this study explicitly defines pores as local dilations and throats as local constrictions [*Raeini et al.*, 2017]. In terms of the associated capillary energy, pores should locally be less favourable places for the invading wetting phase to pervade, while throats should be more favourable. Therefore, we tracked the invasion of the wetting phase in these locations in the experiment and the model, using the same network extraction on both. We define filling in the experiment as events where the image shows a change in oc-

cupancy, such that the voxels associated with the maximal sphere centred on a pore or throat first become occupied principally by the wetting phase in the segmented image.

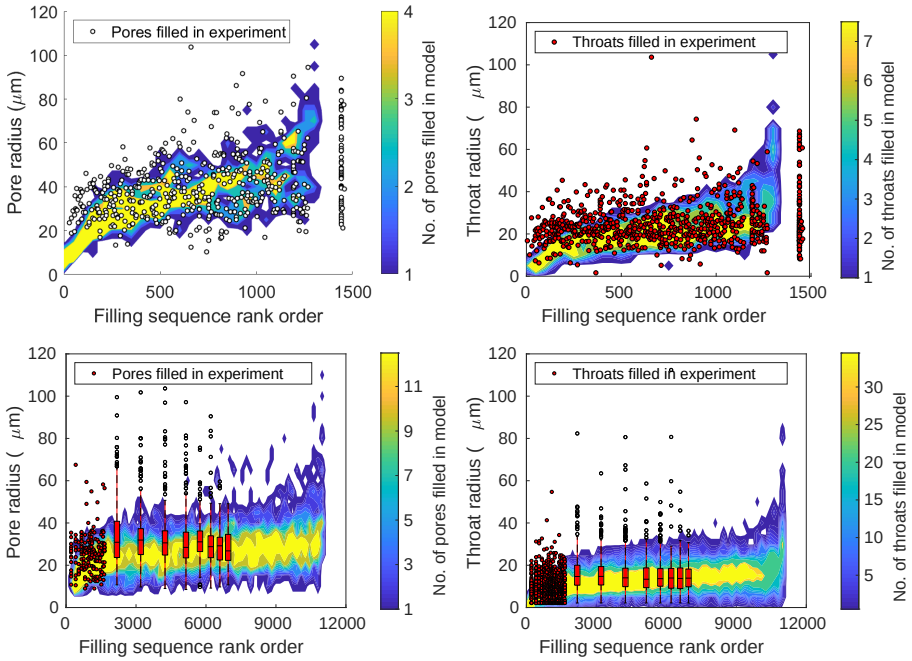

Figure 3. Pore and throat filling sizes in the the model and the experiment for Ketton (top row) and Gildehauser (bottom row) matched well, although there is a tendency for a small number of larger elements to be filled in the experiment and not by the model. Dots and box plots (for time steps where many network elements were invaded at the same time) present the radii of pores and throats filled with the invading wetting phase during the experiment in rank order. The contour plots show the pore or throat radii filled in the model.

Figure 3 shows the radii of pores and throats that were invaded during the experiment as a function of their rank order in the filling sequence. In general, pores and throats of similar sizes were filled throughout the filling sequence in the experiment and the model. In both cases, filling did not strictly happen in order of increasing radius due to the occurrence of the three types of filling (snap-off, piston-like advance and cooperative pore filling) and the variation in pore and throat shapes. A small number of pores and throats with large radii were filled in the experiment, but not in the simulations. This could be related to geometry simplifications in the network model, to local variations in wettability [*AlRatrout et al.*, 2018], or to viscous and/or inertial effects which are not captured in the quasi-static PNM. A decrease of the local capillary pressure caused by the latter two effects may have led to the invasion of pores with larger characteristic size than predicted by the quasi-static model.

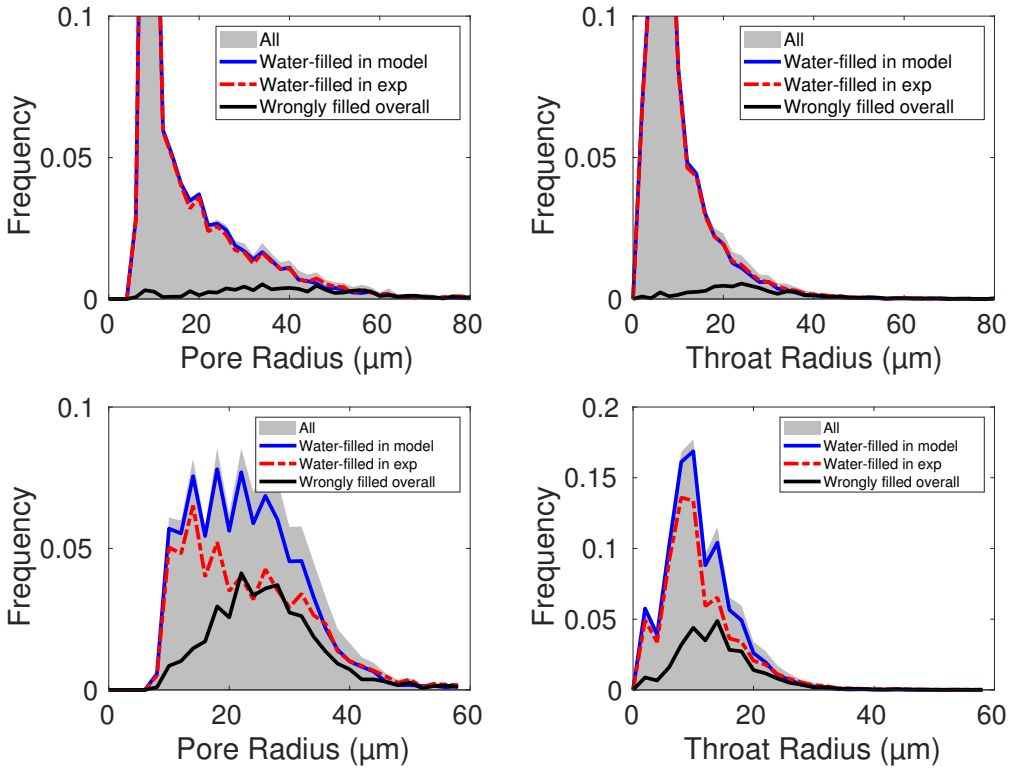

Figure 4. Pore and throat sizes that are filled with water at the end of imbibition, for Ketton (top row) and Gildehauser (bottom row). The black line indicates the frequency of pore and throat sizes that were filled with fluid in the model different than in the experiment.

Figure 4 shows the size distribution of the water-filled pores and throats in the experiments and the model after imbibition, and indicates pores and throats filled with a fluid in the model different from the experiment, similar to *Bultreys et al.* [2018] and *Øren et al.* [2019]. In the Ketton experiment both model and experiment reached residual saturation. There is a very close agreement, with a filling discrepancy of 9 % in the pores and 6 % in the throats (the percentage of pores or throats that were filled with a different fluid in the model as in the experiment).

The Gildehauser experiment did not reach the residual saturation in the experimental field of view, and therefore we compared the simulated fluid distribution with the same saturation as the final state in the experiment. The model overpredicted the number of water-filled pores and throats, resulting in a filling discrepancy of 30 % in the throats and 38 % in the pores. This is explained by the fact that the simulation was stopped at the same saturation as the experiment, while a number of large pores were filled earlier in the experiment than in the model (Figure 3). A previous study showed filling discrepancies of 18 % and 21 % for PNM simulations compared to steady-state Bentheimer experiments at the end of imbibition [*Bultreys et al.*, 2018], and a standard deviation of up to 25 % on the pore occupancy for the intermediately-sized pores in repeated experiments. A different study on Paaratte sandstone found filling discrepancies of 15 % and 13 % [*Øren et al.*, 2019].

The validation of pore and throat filling sizes presented here improves on the approach in *Bultreys et al.* [2018] and *Øren et al.* [2019] because it took the dynamics of the filling process into account. Overall, a more favourable agreement was found here than in *Bultreys et al.* [2018] due to the use of a different cooperative pore filling algorithm [*Ruspini et al.*, 2017] and initial and boundary conditions that more closely resembled those of the experiment. The cooperative pore filling algorithm developed by *Ruspini et al.* [2017] is a significant improvement over the previously available algorithms because it accounts for the local geometry of the surrounding throats to assign the capillary invasion pressures.

In repeated drainage-imbibition experiments on Bentheimer, the standard deviation of the filling state was found to be up to 25 % for the most variable pores, while the large-scale behaviour did not vary significantly [*Bultreys et al.*, 2018]. The filling discrepancy between the PNM simulation and the experiment is thus of similar magnitude to the difference between two repeat experiments that are macroscopically nearly indistinguishable.

Connectivity

The upscaled flow characteristics are strongly influenced by the phase connectivity [*Hilfer*, 2006], which can be characterized by the Euler characteristic [*Armstrong et al.*, 2016; *Schlüter et al.*, 2016]. We compared the evolution of the Euler characteristic during imbibition in the model and the experiment (Figure 5). A consistent comparison to the simulations was achieved by mapping the experimental distributions on the PNM and calculating the Euler characteristic there. The experimental trend is consistent with direct image-based calculations [*Alpak et al.*, 2018].

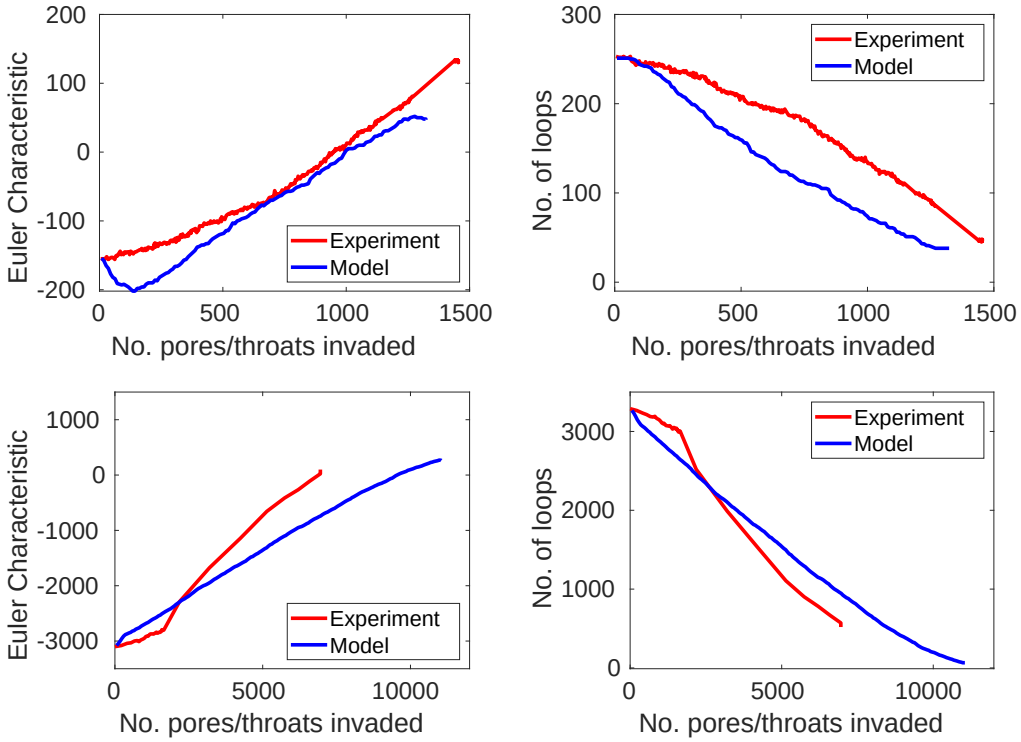

Figure 5. Comparison of the evolution of the non-wetting phase Euler characteristic in the experiment and in the model (left) and the amount of loops in the non-wetting phase (right), for Ketton (top) and Gildehauser (bottom). A large negative Euler characteristic indicates that the non-wetting phase is well connected with many loops in the structure.

Figure 5 shows that magnitude and trends of the Euler characteristic are correctly represented by the model. There are, however, some discrepancies. In the Ketton simulation the model shows a local minimum at the start of imbibition. This is caused by an image processing artifact: small pores that were wrongly identified as non-wetting-filled after drainage.

The effect of this on the Euler characteristic was partly compensated by redundant loops in the modelled non-wetting phase distribution being removed too quickly. The latter may have been caused by a mismatch in the amount of cooperative pore filling compared to snap-off between the simulation and the experiment, due to geometric simplifications in the model. Imbibition in Ketton is more sensitive to cooperative pore filling than most other rock samples, due to Ketton's pore structure resembling that of a bead pack [*Ruspini et al.*, 2017]. In this particular case, the model may therefore overestimate the amount of capillary trapping.

In the Gildehauser case, the Euler characteristic increased more quickly in the experiment than in the model. In the experiment, there was a change in the slope of the Euler characteristic and the number of loops after approximately 1600 pores and throats were filled. This was likely related to the occurrence of two different filling regimes observed by *Rücker et al.* [2015]: first pathway flow and film swelling, and then a regime which includes cluster dynamics. This was not reproduced in the model. Furthermore, the faster increase in the experimental Euler characteristic is partly due to misidentification of the fluid occupancy in smaller pores and throats caused by imaging noise in the Gildehauser experiment. This resulted in an excessive amount of small non-wetting phase clusters being detected. However, the average sizes of multi-throat clusters (excluding single-throat clusters to reduce imaging noise) were in fair agreement between the model and the experiment, as were the sizes of the largest non-wetting phase clusters which dominate the flow (see Supporting Information). As will be shown in the next section, the discrepancies discussed here had a limited influence on the flow paths through each fluid.

Flow paths

The filled pore/throat sizes and the connectivity together control the flow paths which are accessible to each fluid, and consequently the relative permeability. We compared the flow paths in the model and the experiment by calculating relative permeabilities on the imaged and the modelled fluid distributions. This relative permeability can be seen as a flow-weighted connectivity of the fluid distributions. Since both the experimental and the modelled results used the same conductivity and volume assignments in pores and throats, mismatches in the presented relative permeabilities can only come from discrepancies in the modelled fluid distributions.

The resulting relative permeabilities indicated a close match between the model and the experiment (Figure 6). This implies that the quasi-static model provided a good estimation of the fluid distribution with respect to its impact on the upscaled flow properties. There were some discrepancies near the end of imbibition in Ketton. This was likely related to a small mismatch of cooperative pore filling versus snap-off, and to the boundary conditions, which were unknown in the experiment due to the limited field of view of the scan. While ganglion dynamics have been seen to play an important role near the residual non-wetting phase saturation in the Gildehauser experiment [*Rücker et al.*, 2015], there is no direct evidence of this in the Ketton dataset. We do not draw conclusions about the behaviour near the end point of imbibition in the Gildehauser case here, as the experiment did not continue until residual non-wetting saturation.

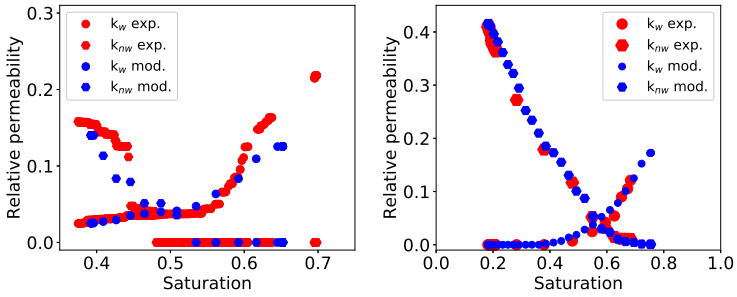

Figure 6. Imbibition relative permeability calculations based on the modelled and the experimental fluid distributions for Ketton (left) and Gildehauser (right) allow to consistently compare the flow paths in the model and the experiment and indicate a good match.

Conclusions

A key question concerning imbibition in permeable materials is how to formulate conceptual models that decrease the degrees of freedom compared to an explicit description, while still capturing the salient behaviour of the process. Quasi-static PNMs abstract the process by simplifying the local pore shapes and by assuming that capillary forces are dominant, allowing imbibition to be described as a sequence of simple pore and throat filling processes. However, one of the main problems has been validation: the complex relation between the fluid occupancy of the system and the experimentally measured properties (e.g. relative permeability) typically used for validation makes it difficult to understand the origin and gener-

ality of any observed (mis-)match [*Sorbie and Skauge*, 2011; *Bondino et al.*, 2012; *Bultreys et al.*, 2018].

The analysis we have developed here allowed the comparison of pore-scale experimental data to a quasi-static PNM with minimal influence from anything but the fluid distributions. This indicated that the quasi-static assumption provided a good approximation of the order in which pores with different sizes were invaded. The model did misinterpret the filling behaviour of some larger pores, and overestimated the amount of loop-breaking in the non-wetting phase. However, the pores and throats causing these discrepancies showed to be of minor importance for the flow paths, which closely matched the experiments.

The conclusion is that an abstracted, conceptually simple model based on quasi-static physics *can* give a good first order approximation of continuum scale properties such as relative permeability, at least in strongly-wetted rocks with relatively homogeneous pore structures and at low capillary numbers. Whether or not it *does*, depends on model implementation (e.g. volume and conductivity assignment) and accurate input concerning pore geometry and advancing contact angles. These less fundamental considerations are outside the scope of this study.

In summary, PNMs as a concept appear a valuable starting point for building conceptual models. However, it must be stressed that more validation needs to point out whether this holds in circumstances where more influence of ganglion dynamics has been observed or can be expected, e.g. near the end of imbibition [*Rücker et al.*, 2015], in intermediate / mixed-wet samples [*Zou et al.*, 2018] and in samples with very wide pore size distributions.

Acknowledgements

Shehadeh Masalmeh and Ove Bjørn Wilson (Shell) are gratefully acknowledged for pointing out the need for this work and putting us on the right path to executing it. Apostolos Georgiadis, Matthias Appel, Xudong Jing and Justin Freeman (Shell) are thanked for valuable discussions on this work. Shell is acknowledged for financial support through the Digital Rocks Programme at Imperial College London, and for permission to publish this paper. Tom Bultreys is currently a postdoctoral fellow of the Research Foundation - Flanders (FWO) and acknowledges its support under grant 12X0919N. The experimental data in this manuscript is freely available via the references in the Materials and Methods section. The

simulation data is made available through the Open Science Foundation (Note: this will be made public with a DOI at time of publication):

https://osf.io/h6sqt/?view_only=10a17e75ba78461da4e84fbb20f65ee1

References

Aghaei, A., and M. Piri (2015), Direct pore-to-core up-scaling of displacement processes: Dynamic pore network modeling and experimentation, *Journal of Hydrology*, *522*, 488–509, doi:10.1016/j.jhydrol.2015.01.004.

Alpak, F., S. Berg, and I. Zacharoudiou (2018), Prediction of Fluid Topology and Relative Permeability in Imbibition in Sandstone Rock by Direct Numerical Simulation, *Advances in Water Resources*, (June), doi:10.1016/j.advwatres.2018.09.001.

AlRatrout, A., M. J. Blunt, and B. Bijeljic (2018), Wettability in complex porous materials, the mixed-wet state, and its relationship to surface roughness, *Proceedings of the National Academy of Sciences*, *115*(36), 8901–8906, doi:10.1073/pnas.1803734115.

Andrew, M., B. Bijeljic, and M. J. Blunt (2014), Pore-scale contact angle measurements at reservoir conditions using X-ray microtomography, *Advances in Water Resources*, *68*, 24–31, doi:10.1016/j.advwatres.2014.02.014.

Andrew, M., H. Menke, M. J. Blunt, and B. Bijeljic (2015), The Imaging of Dynamic Multiphase Fluid Flow Using Synchrotron-Based X-ray Microtomography at Reservoir Conditions, *Transport in Porous Media*, *110*(1), 1–24, doi:10.1007/s11242-015-0553-2.

Armstrong, R. T., J. E. Mcclure, M. A. Berrill, M. Rücker, S. Schlüter, and S. Berg (2016), Beyond Darcy's law: The role of phase topology and ganglion dynamics for two-fluid flow, *Physical Review E*, *94*(043113), doi:10.1103/PhysRevE.94.043113.

Atteia, O., E. Del Campo Estrada, and H. Bertin (2013), Soil flushing: a review of the origin of efficiency variability, *Reviews in Environmental Science and Bio/Technology*, *12*(4), 379–389, doi:10.1007/s11157-013-9316-0.

Berg, S., H. Ott, S. a. Klapp, A. Schwing, R. Neiteler, N. Brussee, A. Makurat, L. Leu, F. Enzmann, J.-O. Schwarz, M. Kersten, S. Irvine, and M. Stampanoni (2013), Real-time 3D imaging of Haines jumps in porous media flow, *Proceedings of the National Academy of Sciences*, *110*(10), 3755–3759, doi:10.1073/pnas.1221373110.

Berg, S., M. Rücker, H. Ott, A. Georgiadis, H. van der Linde, F. Enzmann, M. Kersten, R. Armstrong, S. de With, J. Becker, and A. Wiegmann (2016), Connected pathway rel-

ative permeability from pore-scale imaging of imbibition, *Advances in Water Resources*, *90*, 24–35, doi:10.1016/j.advwatres.2016.01.010.

Berg, S., R. Armstrong, and A. Wiegmann (2018), Micro-CT scans of a fast synchrotron-based micro-CT flow experiment performed in Gildehauser sandstone rock., doi:10.17612/P7WW95.

Berge, C. (2001), *The theory of graphs*, Courier Dover Publications.

Bickle, M. J. (2009), Geological carbon storage, *Nature Geoscience*, *2*, 815–818, doi:10.1038/ngeo687.

Blunt, M., M. King, and H. Scher (1992), Simulation and theory of two-phase flow in porous media, *Physical Review A*, *46*(12), 7680–7699, doi:10.1103/PhysRevA.46.7680.

Blunt, M. J. (2017), *Multiphase Flow in Permeable Media: A Pore-Scale Perspective*, Cambridge University Press, Cambridge, UK.

Blunt, M. J., B. Bijeljic, H. Dong, O. Gharbi, S. Iglauer, P. Mostaghimi, A. Paluszny, and C. Pentland (2013), Pore-scale imaging and modelling, *Advances in Water Resources*, *51*, 197–216, doi:10.1016/j.advwatres.2012.03.003.

Bondino, I., G. Hamon, W. Kallel, and D. Kachuma (2012), Relative permeabilities from simulation in 3D rock models and equivalent pore networks: critical review and way forward, in *Int. Symp. Soc. Core Analysts*, Society for Core Analysts, Society of Core Analysts, Aberdeen, Scotland.

Bultreys, T., W. De Boever, and V. Cnudde (2016a), Imaging and image-based fluid transport modeling at the pore scale in geological materials: A practical introduction to the current state-of-the-art, *Earth-Science Reviews*, *155*, 93–128, doi:10.1016/j.earscirev.2016.02.001.

Bultreys, T., M. N. M. A. Boone, M. N. M. A. Boone, T. De Schryver, B. Masschaele, L. Van Hoorebeke, and V. Cnudde (2016b), Fast laboratory-based micro-computed tomography for pore-scale research: Illustrative experiments and perspectives on the future, *Advances in Water Resources*, *95*, 341–351, doi:10.1016/j.advwatres.2015.05.012.

Bultreys, T., Q. Lin, Y. Gao, A. Q. Raeini, A. AlRatrout, B. Bijeljic, and M. J. Blunt (2018), Validation of model predictions of pore-scale fluid distributions during two-phase flow, *Physical Review E*, *97*(5), 053,104, doi:10.1103/PhysRevE.97.053104.

Ferrari, A., and I. Lunati (2013), Direct numerical simulations of interface dynamics to link capillary pressure and total surface energy, *Advances in Water Resources*, *57*, 19–31, doi:10.1016/j.advwatres.2013.03.005.

Ferrari, A., J. Jimenez-Martinez, T. L. Borgne, Y. Méheust, and I. Lunati (2015), Challenges in modeling unstable two-phase flow experiments in porous micromodels, *Water Resources Research*, *51*(3), 1381–1400, doi:10.1002/2014WR016384.

Gao, Y., Q. Lin, B. Bijeljic, and M. J. Blunt (2017), X-ray Microtomography of Intermittency in Multiphase Flow at Steady State Using a Differential Imaging Method, *Water Resources Research*, *53*(12), 10,274–10,292, doi:10.1002/2017WR021736.

Gostick, J., M. Aghighi, J. Hinebaugh, T. Tranter, M. A. Hoeh, H. Day, B. Spellacy, M. H. Sharqawy, A. Bazylak, A. Burns, W. Lehnert, and A. Putz (2016), OpenPNM: A Pore Network Modeling Package, *Computing in Science & Engineering*, *18*(4), 60–74, doi:10.1109/MCSE.2016.49.

Herring, A. L., E. J. Harper, L. Andersson, A. Sheppard, B. K. Bay, and D. Wildenschild (2013), Effect of fluid topology on residual nonwetting phase trapping: Implications for geologic CO2 sequestration, *Advances in Water Resources*, *62*, 47–58, doi:10.1016/j.advwatres.2013.09.015.

Hilfer, R. (2006), Macroscopic capillarity and hysteresis for flow in porous media, *Physical Review E*, *73*(016307), doi:10.1103/PhysRevE.73.016307.

Hilfer, R., R. T. Armstrong, S. Berg, A. Georgiadis, and H. Ott (2015), Capillary saturation and desaturation, *Physical Review E - Statistical, Nonlinear, and Soft Matter Physics*, *92*(6), 1–11, doi:10.1103/PhysRevE.92.063023.

Jerauld, G. R., J. Fredrich, N. Lane, Q. Sheng, B. Crouse, D. M. Freed, A. Fager, and R. Xu (2017), Validation of a Workflow for Digitally Measuring Relative Permeability, *SPE Abu Dhabi International Petroleum Exhibition & Conference*, doi:10.2118/188688-MS.

Joekar-Niasar, V., and S. M. Hassanizadeh (2012), Analysis of Fundamentals of Two-Phase Flow in Porous Media Using Dynamic Pore-Network Models: A Review, *Critical Reviews in Environmental Science and Technology*, *42*(18), 1895–1976, doi:10.1080/10643389.2011.574101.

Khishvand, M., M. Akbarabadi, and M. Piri (2016), Micro-scale experimental investigation of the effect of flow rate on trapping in sandstone and carbonate rock samples, *Advances in Water Resources*, *94*, 379–399, doi:10.1016/j.advwatres.2016.05.012.

Lenormand, R., C. Zarcone, and A. Sarr (1983), Mechanisms of the displacement of one fluid by another in a network of capillary ducts, *Journal of Fluid Mechanics*, *135*, 337, doi:10.1017/S0022112083003110.

Ling, B., J. Bao, M. Oostrom, I. Battiato, and A. M. Tartakovsky (2017), Modeling variability in porescale multiphase flow experiments, *Advances in Water Resources*, *105*, 29–38, doi:10.1016/j.advwatres.2017.04.005.

Liu, Y.-Y., J.-J. Slotine, and A.-L. Barabasi (2013), Observability of complex systems, *Proceedings of the National Academy of Sciences*, *110*(7), 2460–2465, doi:10.1073/pnas.1215508110.

Masalmeh, S. K., X. Jing, S. Roth, C. Wang, H. Dong, and M. Blunt (2015), Towards Predicting Multi-Phase Flow in Porous Media Using Digital Rock Physics : Workflow to Test the Predictive Capability of Pore-Scale Modeling Outline of the Workflow, in *Abu Dhabi International Petroleum Exhibition and Conference*, Society of Petroleum Engineers, Abu Dhabi, UAE, doi:10.2118/177572-MS.

McClure, J. E., R. T. Armstrong, M. A. Berrill, S. Schlüter, S. Berg, W. G. Gray, and C. T. Miller (2018), Geometric state function for two-fluid flow in porous media, *Physical Review Fluids*, *3*(8), 084,306, doi:10.1103/PhysRevFluids.3.084306.

Meakin, P., and A. M. Tartakovsky (2009), Modeling and simulation of pore-scale multiphase fluid flow and reactive transport in fractured and porous media, *Reviews of Geophysics*, *47*(3), RG3002, doi:10.1029/2008RG000263.

Øren, P., L. Ruspini, M. Saadatfar, R. Sok, M. Knackstedt, and A. Herring (2019), In-situ pore-scale imaging and image-based modelling of capillary trapping for geological storage of CO2, *International Journal of Greenhouse Gas Control*, *87*, 34–43, doi:10.1016/j.ijggc.2019.04.017.

Øren, P.-E., S. Bakke, and O. J. Arntzen (1998), Extending Predictive Capabilities to Network Models, *SPE Journal*, *3*(04), 324–336, doi:10.2118/52052-PA.

Raeini, A. Q., B. Bijeljic, and M. J. Blunt (2017), Generalized network modeling: Network extraction as a coarse-scale discretization of the void space of porous media, *Physical Review E*, *96*(1), 013,312, doi:10.1103/PhysRevE.96.013312.

Reynolds, C. A., H. Menke, M. Andrew, M. J. Blunt, and S. Krevor (2017), Dynamic fluid connectivity during steady-state multiphase flow in a sandstone, *Proceedings of the National Academy of Sciences*, *114*(31), 8187–8192, doi:10.1073/pnas.1702834114.

Rücker, M., S. Berg, R. T. Armstrong, A. Georgiadis, H. Ott, A. Schwing, R. Neiteler, N. Brussee, A. Makurat, L. Leu, M. Wolf, F. Khan, F. Enzmann, and M. Kersten (2015), From connected pathway flow to ganglion dynamics, *Geophysical Research Letters*, *42*(10), 3888–3894, doi:10.1002/2015GL064007.

549 Ruspini, L. C., R. Farokhpoor, and P. E. Øren (2017), Pore-scale modeling of capillary trap-
550 ping in water-wet porous media: A new cooperative pore-body filling model, *Advances in*
551 *Water Resources*, *108*, 1–14, doi:10.1016/j.advwatres.2017.07.008.
552 Scanziani, A., K. Singh, M. J. Blunt, and A. Guadagnini (2017), Automatic method for es-
553 timation of in situ effective contact angle from X-ray micro tomography images of two-
554 phase flow in porous media, *Journal of Colloid and Interface Science*, *496*, 51–59, doi:
555 10.1016/j.jcis.2017.02.005.
556 Schlüter, S., S. Berg, M. Rücker, R. T. Armstrong, H.-J. Vogel, R. Hilfer, and D. Wilden-
557 schild (2016), Pore-scale displacement mechanisms as a source of hysteresis for
558 two-phase flow in porous media, *Water Resources Research*, *52*(3), 2194–2205, doi:
559 10.1002/2015WR018254.
560 Schlüter, S., S. Berg, T. Li, H.-J. Vogel, and D. Wildenschild (2017), Time scales of relax-
561 ation dynamics during transient conditions in two-phase flow, *Water Resources Research*,
562 *53*(6), 4709–4724, doi:10.1002/2016WR019815.
563 Shams, M., A. Q. Raeini, M. J. Blunt, and B. Bijeljic (2018), A numerical model of two-
564 phase flow at the micro-scale using the volume-of-fluid method, *Journal of Computational*
565 *Physics*, *357*, 159–182, doi:10.1016/j.jcp.2017.12.027.
566 Singh, K., B. Bijeljic, and M. J. Blunt (2016), Imaging of oil layers, curvature, and contact
567 angle in a mixed-wet and a water-wet carbonate rock, *Water Resources Research*, pp. n/a–
568 n/a, doi:10.1002/2015WR018072.
569 Singh, K., H. Menke, M. Andrew, Q. Lin, C. Rau, M. J. Blunt, and B. Bijeljic (2017), Dy-
570 namics of snap-off and pore-filling events during two-phase fluid flow in permeable media,
571 *Scientific Reports*, *7*(1), 5192, doi:10.1038/s41598-017-05204-4.
572 Singh, K., H. Menke, M. Andrew, C. Rau, B. Bijeljic, and M. J. Blunt (2018), Time-resolved
573 synchrotron X-ray micro-tomography datasets of drainage and imbibition in carbonate
574 rocks, *Scientific Data*, *5*, 180,265, doi:10.1038/sdata.2018.265.
575 Sorbie, K. S., and A. Skauge (2011), Can network modelling predict two-phase flow func-
576 tions?, in *Int. Symp. Soc. Core Analysts*, 1956, Society of Core Analysts, Austin, USA.
577 Valvatne, P. H., and M. J. Blunt (2004), Predictive pore-scale modeling of two-
578 phase flow in mixed wet media, *Water Resources Research*, *40*(7), n/a–n/a, doi:
579 10.1029/2003WR002627.
580 Wildenschild, D., and A. P. Sheppard (2013), X-ray imaging and analysis techniques for
581 quantifying pore-scale structure and processes in subsurface porous medium systems, *Ad-*

582 *vances in Water Resources*, *51*(0), 217–246, doi:10.1016/j.advwatres.2012.07.018.
583 Wilkinson, D., and J. F. Willemsen (1983), Invasion percolation: a new form of percola-
584 tion theory, *Journal of Physics A: Mathematical and General*, *16*(14), 3365–3376, doi:
585 10.1088/0305-4470/16/14/028.
586 Youssef, S., H. Deschamps, J. Dautriat, E. Rosenberg, R. Oughanem, E. Maire, and
587 R. Mokso (2013), 4D Imaging of fluid flow dynamics in natural porous media with ultra-
588 fast X-ray microtomography, in *Int. Symp. Soc. Core Analysts*, Society of Core Analysts,
589 Napa Valley, USA.
590 Zhao, B., C. W. MacMinn, and R. Juanes (2016), Wettability control on multiphase flow
591 in patterned microfluidics, *Proceedings of the National Academy of Sciences*, *113*(37),
592 10,251–10,256, doi:10.1073/pnas.1603387113.
593 Zou, S., R. T. Armstrong, J.-y. Arns, C. H. Arns, and F. Hussain (2018), Experimen-
594 tal and Theoretical Evidence for Increased Ganglion Dynamics During Fractional
595 Flow in Mixed-Wet Porous Media, *Water Resources Research*, *54*(5), 3277–3289, doi:
596 10.1029/2017WR022433.